Earth and Planetary Science Letters 493 (2018) 12–24

Contents lists available at ScienceDirect

Earth and Planetary Science Letters

www.elsevier.com/locate/epsl

Origin of spectacular fields of submarine sediment waves around volcanic islands

Ed L. Pope [a,*], Martin Jutzeler [b], Matthieu J.B. Cartigny [c], James Shreeve [d,e,f], Peter J. Talling [c], Ian C. Wright [g], Richard J. Wysoczanski [h]

[a] Department of Geography, Durham University, Science Laboratories, South Road, Durham, DH1 3LE, UK
[b] School of Physical Sciences and Centre of Excellence in Ore Deposits (CODES), University of Tasmania, Hobart TAS 7001, Australia
[c] Departments of Earth Science and Geography, Durham University, Science Laboratories, South Road, Durham, DH1 3LE, UK
[d] National Oceanography Centre Southampton, European Way, Southampton, SO14 3ZH, UK
[e] School of Ocean and Earth Science, University of Southampton, National Oceanography Centre Southampton, European Way, Southampton, Hampshire, SO14 3ZH, UK
[f] Geotek Ltd, 4 Sopwith Way, Drayton Fields, Daventry, NN11 8PB, UK
[g] Vice Chancellor's Office, University of Canterbury, Private Bag 4800, Christchurch 8140, New Zealand
[h] National Institute of Water and Atmospheric Research, PO BOX 14-901, Wellington, New Zealand

ARTICLE INFO

Article history:
Received 23 June 2017
Received in revised form 6 April 2018
Accepted 12 April 2018
Available online xxxx
Editor: T.A. Mather

Keywords:
volcanic islands
landslides
eruption-fed turbidity currents
geohazards
submarine bedforms

ABSTRACT

Understanding how large eruptions and landslides are recorded by seafloor morphology and deposits on volcanic island flanks is important for reconstruction of volcanic island history and geohazard assessment. Spectacular fields of bedforms have been recognised recently on submerged flanks of volcanic islands at multiple locations worldwide. These fields of bedforms can extend over 50 km, and individual bedforms can be 3 km in length and 150 m in height. The origin of these bedform fields, however, is poorly understood. Here, we show that bedforms result from eruption-fed supercritical density flows (turbidity currents) in some locations, but most likely rotational landslides at other locations. General criteria are provided for distinguishing between submarine bedforms formed by eruptions and landslides, and emphasise a need for high resolution seismic datasets to prevent ambiguity. Bedforms associated with rotational landslides have a narrower source, with a distinct headscarp, they are more laterally confined, and internal bedform structure does not suggest upslope migration of each bedform. Eruption-fed density currents produce wide fields of bedforms, which extend radially from the caldera. Internal layers imaged by detailed seismic data show that these bedforms migrated up-slope, indicating that the flows that produced them were Froude supercritical. Due to the low density contrast between interstitial fluid and sediment, the extent and dimensions of submarine eruption-fed bedforms is much greater than those produced by pyroclastic density currents on land.

1. Introduction

Silicic caldera-forming eruptions and landslides on volcanic islands represent some of the highest sediment flux events on Earth. They can transport tens to hundreds of cubic kilometres of material (Pyle, 1995; Hunt et al., 2013), most likely over a few hours to days. Both caldera-forming eruptions and landslides are extremely hazardous for local populations, and can generate far-travelling tsunami that effect more widespread distal coastlines. Explosive eruptions produce large amounts of material that can be rapidly transferred from the vent to submarine slopes and basins via volcaniclastic density flows (Cas and Wright, 1991; Allen et al., 2012). The landslides that occur on volcanic flanks can be unusually large, and involve both the subaerial and submarine domains of the edifice (White, 2000; Masson et al., 2006; Watt et al., 2012). Further, they can also evacuate material to surrounding basins through density flows (Le Friant et al., 2015; Watt et al., 2015). It is therefore important to understand how eruptions and landslides are recorded on submerged volcanic island flanks, and to distinguish between caldera-forming density current deposits and large submarine landslides as they pose distinctly different types of hazards.

Worldwide, recent work has recognised extensive fields of bedforms on submerged volcanic island flanks (Wright et al., 2006; Silver et al., 2009; Gardner, 2010; Leat et al., 2010 and references

* Corresponding author.
E-mail address: Edward.Pope@durham.ac.uk (E.L. Pope).

https://doi.org/10.1016/j.epsl.2018.04.020

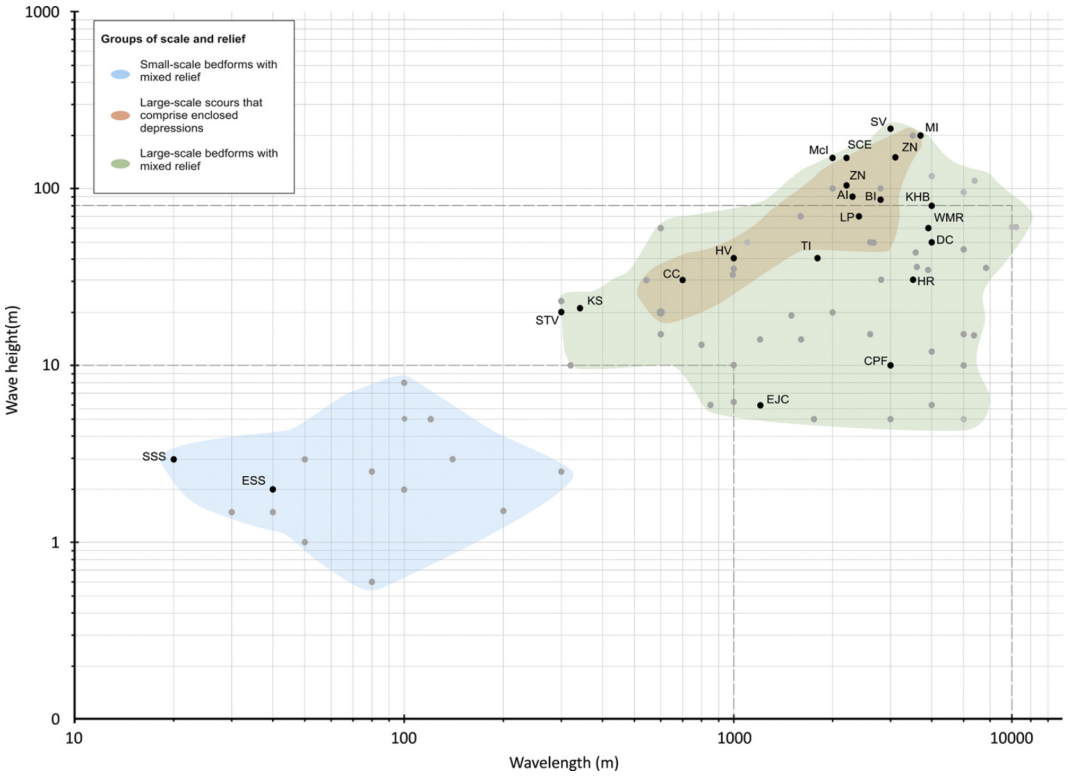

Fig. 1. Logarithmic plot of wavelength versus wave height for global submarine bedform examples. Black points indicate volcanic setting. Grey points indicate other settings. AI – Adventure Island; BI – Bristol Island; CC – Cilaos Canyons; CPF – Cilaos Proximal Fan; DC – Dakataua Caldera, New Britain; EJC – El Julan Channel; ESS – Etang-Salé Sector, La Reunion; HV – Haleakala Volcano; HR – Hawaiian Ridge; KS – Kahouanne Seamounts; KHB – Kimbe and Hixon Bay; LP – La Palma; McI – Macauley Island; MI – Montagu Island; SCE – South Candlemas Embayment; STV – Stromboli Volcano; SV – Sumisu Volcano; TI – Tolokiwa; WMR – West Mariana Ridge; ZN – Zavodovski. Adapted from Symons et al. (2016). See Symons et al. (2016) for full reference list. (For interpretation of the colours in the figure(s), the reader is referred to the web version of this article.)

therein) that are some of the largest amplitude bedforms yet documented on the seafloor (Fig. 1; Symons et al., 2016). 'Bedform' is used here to denote undulations without any reference about their origin. These undulating areas of seafloor can extend for over 50 km, and individual bedforms have wavelengths up to 3 km, and wave heights of 10–150 m. However, the origin of these bedforms is uncertain. As shown by debate over the origin of such bedforms in non-volcanic settings, they can potentially result from both rotational landslide blocks and remoulding of the seabed by density flows (Lee et al., 2002).

The origin of these submarine bedforms is also particularly interesting because they are larger than any known bedforms on the subaerial flanks of volcanoes. Identified submarine bedform fields are extensive and contain large amplitude bedforms. In contrast, subaerial volcanic flank bedform fields are less extensive and contain smaller-scale bedforms associated with terrestrial dilute pyroclastic density currents (e.g. Sigurdsson et al., 1987; Branney and Kokelaar, 2002; Brown and Branney, 2004), or irregular hummocky terrain formed by debris avalanches and landslides (e.g. Crandell et al., 1984; Cas and Wright, 1991). We therefore seek to understand what the contrasting dimensions of submarine and subaerial bedform fields can tell us about important general differences between subaerial and submarine volcanic mass flows (Moorhouse and White, 2016).

Eruption-fed submarine density flows sourced from either subaerial or submarine vents can be initiated by either collapse of eruption columns or disintegration of active lava domes (Cas and Wright, 1991; Kokelaar and Busby, 1992; Head and Wilson, 2003). Sediment waves (cyclic steps, anti-dunes, etc.) and scours are thought to be the submarine slope expression of these flows (Kostic and Parker, 2006; Spinewine et al., 2009; Cartigny et al., 2011).

Failure of submarine volcanic shelves and slopes can result from earthquakes, edifice uplift, magma intrusion and extrusion or the sudden accumulation of large volumes of pyroclasts during volcanic eruptions (Watt et al., 2014). These failures commonly affect deep substrate and terminate proximally at steep headwall scars (Masson et al., 2006). Landslide deposits include rotated domains, huge individual blocks, and various types of density flow deposits (Masson et al., 2006; Watt et al., 2015). Landslide deposits made up of rotated blocks can form an undulating seafloor that shares some surficial similarities to sediment waves emplaced by eruption-fed density flows (Lee et al., 2002; Leat et al., 2010). This can make it difficult to distinguish landslide block and sediment flow deposits, as previously noted for bedforms in non-volcanic sites (Lee et al., 2002).

Our lack of understanding of proximal submarine volcanic slope deposits is a consequence of the lack of attention that they have received. Basin records of volcanic deposits are relatively well understood from the rock record (Trofimovs et al., 2006; Allen and McPhie, 2009; Jutzeler et al., 2014a) and ocean drilling (Nishimura et al., 1991; Le Friant et al., 2015; Busby et al., 2017). In contrast, scientific drilling has never been successful in proximal environments (ODP135; IODP340), high-resolution geophysical data is limited (Gardner, 2010; Leat et al., 2010; Casalbore et al., 2014a, 2014b), and extensive subaerial exposures of these deposits are rare and often incomplete (Cas and Wright, 1991; Allen and McPhie, 2009).

1.1. Aims

Our overall aim is to understand the origin and wider significance of extensive fields of bedforms on volcanic island flanks, whose occurrence has been recently recognised in locations world-

Table 1
Geomorphic matrix providing general criteria for initial interpretations of whether bedforms are generated by eruption-fed density flows or landslides based on swath bathymetry.

Type	Example Planform Morphology	Characterisitics	Geometry	Interpretation
Type 1 Convex waves	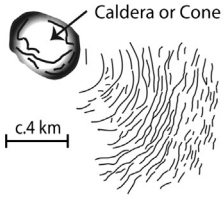	• Convex morphology in planform • Symmetrical to asymmetrical bedforms • Decrease in wavelength and waveheight downslope • Bedforms often bifurcate • Poorly defined lateral margins • No headwall •Positive bathymetric relief over wavefield • Upslope limb is aggradational and downslope limb is erosional to non-depositional	Waveheight: <10 m to 140 m Wavelength: 250 m to 1500 m	Bedforms formed by erutpion-fed density flows
Type 2a - Probable Slope Failure	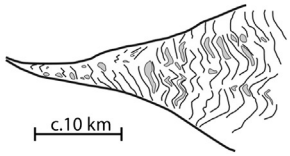	• Linear to zig-zag-like morphology in planform • Symmetrical flat-topped bedforms • Confined by two well defined lateral margins • Arcuate headwall present at shelf break • Little to no change in wave geometry downslope • Waveforms are well-bedded and backward rotated overlying a basal shear surface	Waveheight: 10 m to 100 m Wavelength: c.1000 m	Bedforms are ridges seperated by extentional normal faults, where each sediment block or ridge moves downslope by backward rotation
Type 2b - Probable Slope Failure	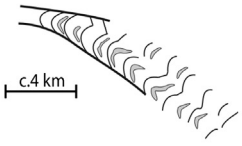	• Concave morphology in planform • Confined by two lateral margins • Symmetrical, flat topped bedforms • Little to no change in bedform geometry downslope • Arcuate headwall present at shelf break • Wavecrest length is the same as the width of the headwall	Waveheight: 50 m to 100 m Wavelength: 370 m to 2000 m	Normal faults are interpreted on the downslope limb of each bedform creating concave ridges and therefore a wavy seafloor
Type 2c - Probable Slope Failure	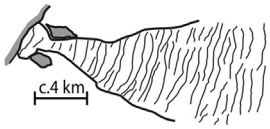	• Concave to linear morphology in planform • Asymmetrical bedforms upslope and symmetrical bedforms downslope • Waveheight and wavelength decreases downslope • Wave crest length increases downslope • Arcuate headwall present at shelf break • Positive bathymetric relief at toe • Well-bedded inclined reflectors within each bedform overlying a chaotic deposit with a basal shear surface	Waveheight: <10 m to 50 m Wavelength: 300 m to 1500 m	Normal faults are interpreted on the downslope limb of each bedform, faults become less continuous and spaced closer together downslope
Type 3 Irregular bedforms	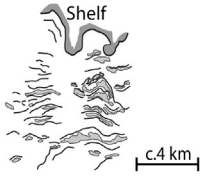	• Irregular shape in planform • Irregular wavelength • Bedforms are parallel to oblique to regional slope • Bedforms are flat topped with no symmetry • No change in bedform geometry downslope • No headwall	Waveheight: 10 m to 25 m Wavelength: 500 m to 1000 m	Normal faults are interpreted to be present within each trough creating low lateral displacement sediment blocks and hence a wavy seafloor

wide. We first consider bedforms on the flanks of Macauley and Raoul Islands in the Kermadec Arc, using particularly detailed seismic surveys and bathymetric mapping data. We provide general criteria for distinguishing between deposits from eruption-fed density flows and landslides (Table 1). We show how these general criteria can help to understand the origin of submarine bedforms at other volcanic islands, and emphasise the need for detailed seismic surveys to reduce ambiguity. We conclude by discussing why similar extensive and well-developed bedforms are not formed subaerially, and what this may tell us about eruption-fed density flows and landslides in general.

2. Geologic setting

Macauley and Raoul Islands are located in the intra-oceanic Kermadec Arc (Fig. 2), being the uppermost subaerial edifices of two active, voluminous submarine stratovolcanoes (Wright et al., 2006; Shane and Wright, 2011; Barker et al., 2013). Onshore Macauley Island, basal deposits comprise basaltic lavas and phreatomagmatic deposits, overlain by the Sandy Bay Tephra Formation and younger basaltic lavas. The 5.7 ka Sandy Bay Tephra is exposed in cliffs 15–100 m high, and is the only confidently known silicic activity related to this volcano (Smith et al., 2003; Shane and Wright, 2011). It is made up of >30 flow units from wet pyroclastic density currents, most likely associated with a large magnitude submarine explosive eruption originated from the now-submarine caldera lying to the northwest of the island (Lloyd et al., 1996; Wright et al., 2006). In contrast, the last 4 ka on Raoul Island are dominated by ~15 km^3 of deposits from multiple dry or phreatomagmatic silicic explosive eruptions linked to two summit calderas (Rotella et al., 2014).

3. Data and methods

Kongsberg EM300 30 kHz multibeam echo-sounder and multichannel seismic data were acquired around Macauley and Raoul Islands during May 2007 onboard RV Tangaroa (TAN0706) and comprises one of the most detailed datasets yet for bedform fields

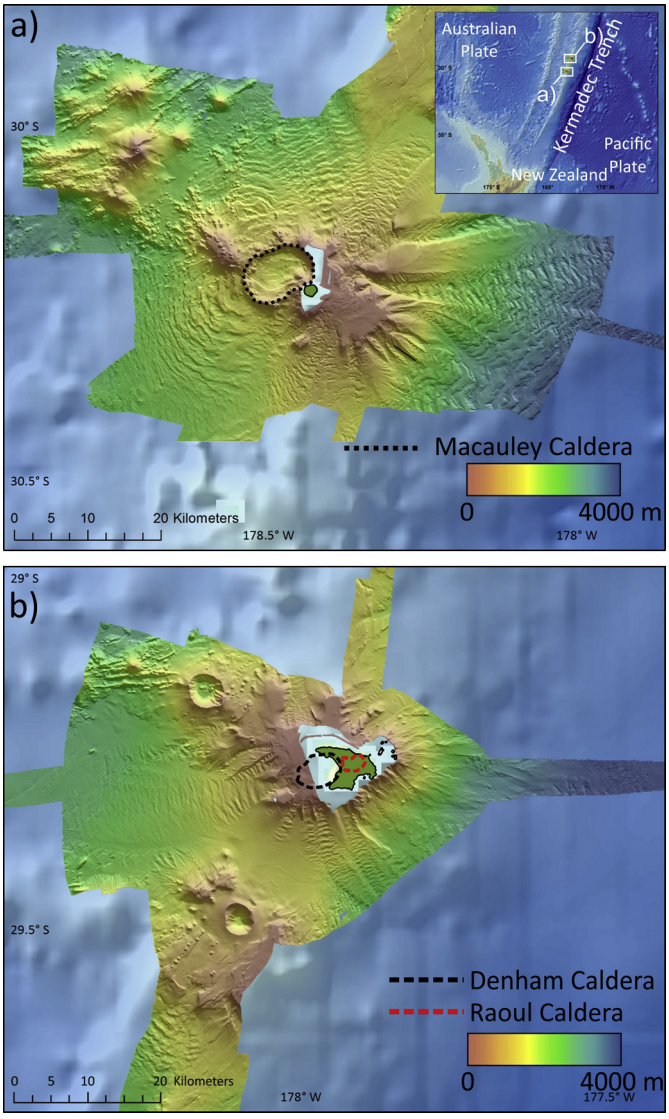

Fig. 2. Map of the study area in the Kermadec Arc, showing extent of detailed bathymetric data acquired in 2007; islands are green areas. a) Map of Macauley Island with Macauley Caldera; inset shows the wider region. b) Map of Raoul Island with Denham and Raoul calderas.

on volcanic island flanks. The multibeam data are gridded to a 25 m cell size with a vertical resolution <1% of water depth. A total of 5 multichannel seismic lines were collected around the two islands using a GI airgun source and a 48 channel streamer. A seismic velocity of 1600 m/s was used to convert two way travel time to depth on all seismic profiles.

Using the bathymetry data, analysis of each bedform field was carried out by first categorising the morphologies of the bedforms within each bedform field. Bedforms were categorised as either convex, concave or linear in planform. Second, the wavelength and wave height of each bedform was catalogued. As part of this analysis, the upslope limb length and downslope limb length of each bedform was recorded; combined with the seismic data, this enabled bedform symmetry to be analysed. Third, the setting of each bedform field was analysed, i.e. are the bedforms confined by a definitive lateral margin or are they unconfined. Fourth, each bedform field was analysed for any notable additional features such as an identifiable headscar. Analysis of the seismic data from the bedform fields was carried out using automatic picking routines in Kingdom Suite. This was followed by manual picking of the seismic reflectors in order to ensure greater accuracy, and identify any artefacts present in the automated routines.

4. Results

4.1. Eruption-fed sediment waves – Macauley Volcano

Repetitive bedforms have developed over large parts of the southwest and northern flanks of Macauley Volcano (Figs. 2 and 3). These semi-continuous undulations extend outwards for over 20 km, from a major break-in-slope formed by the external rim of the submarine caldera. In planform these bedforms have a repetitive convex morphology and have poorly defined lateral margins. The wavelengths of bedforms on the caldera's southern flank decreases downslope from 1500 to 250 m, whilst their amplitude decreases from 140 to 10 m.

Seismic data from the southwest bedform field shows multiple high amplitude reflectors making up a chaotic facies (Figs. 3b, c and 4). Separated from this facies by a stratigraphic unconformity, a series of thin, ordered lower amplitude reflectors are apparent. The lower amplitude reflectors make up the bedforms themselves (Figs. 3 and 4). An internal unconformity is also identifiable within the lower amplitude reflectors. The strength of the reflector that marks this unconformity is highly variable along the seismic line (Fig. 4). Our interpretation of this unconformity is marked by the green line in Figs. 3 and 4, and represents either a change in the seismic character of the reflectors (e.g. an abrupt change in orientation), a truncation of other reflectors, or a specific higher amplitude reflector (see Fig. 4). If this surface represents a significant unconformity, then there are >20 planar reflectors beneath this surface and >30 above.

The planar reflectors below the interpreted unconformity are truncated at high angles on their lee sides (Fig. 4). Each reflector is truncated by the proposed unconformity (Fig. 4f). The upslope limb length of the bedforms in this lower set of reflectors is on average 1.84 times the length of the downslope limb length. The greater upslope limb length of bedforms in the lower set of reflectors defines this set of reflectors as asymmetric.

In comparison, the upper set of reflectors are more clearly defined and well-developed. These reflectors conform to the underlying interpreted unconformity. The reflectors in the upper set have a dome-like apex, and their lee sides are thin but not truncated, instead becoming unresolvable in the seismic data (see Fig. 4b–d). As a result, the upper set of reflectors that make up the bedforms are more symmetrical. The upslope limb is on average only 1.55 times the length of the downslope limb. In some bedforms, some continuous and well-layered reflectors can be traced from one flank to the other, but it is difficult to correlate reflectors between one bedform and the next.

Proximal to the caldera, where the wave amplitudes are greatest, the regular reflectors cut into the chaotic reflector patterns which are thought to represent the underlying substrate. Ponded facies have also developed closest to the break-in-slope indicated by the chaotic reflector patterns on the seismic data (Fig. 4).

The total bulk volume of these bedforms around the whole island is at least ~27.5 km^3, with ~17.5 km^3 on the calderas southern flank, and ~10 km^3 on the northern flank. This volume estimate uses the basal scoped reflector, shown in orange on Fig. 3.

4.1.1. Emplacement mechanism

A number of possible mechanisms exist which could have resulted in the emplacement of the observed bedforms. First, they could be emplaced by poorly confined sediment density flows resulting from the radial collapse of an eruption column. In this instance, each bedform is a consequence of flow interaction with

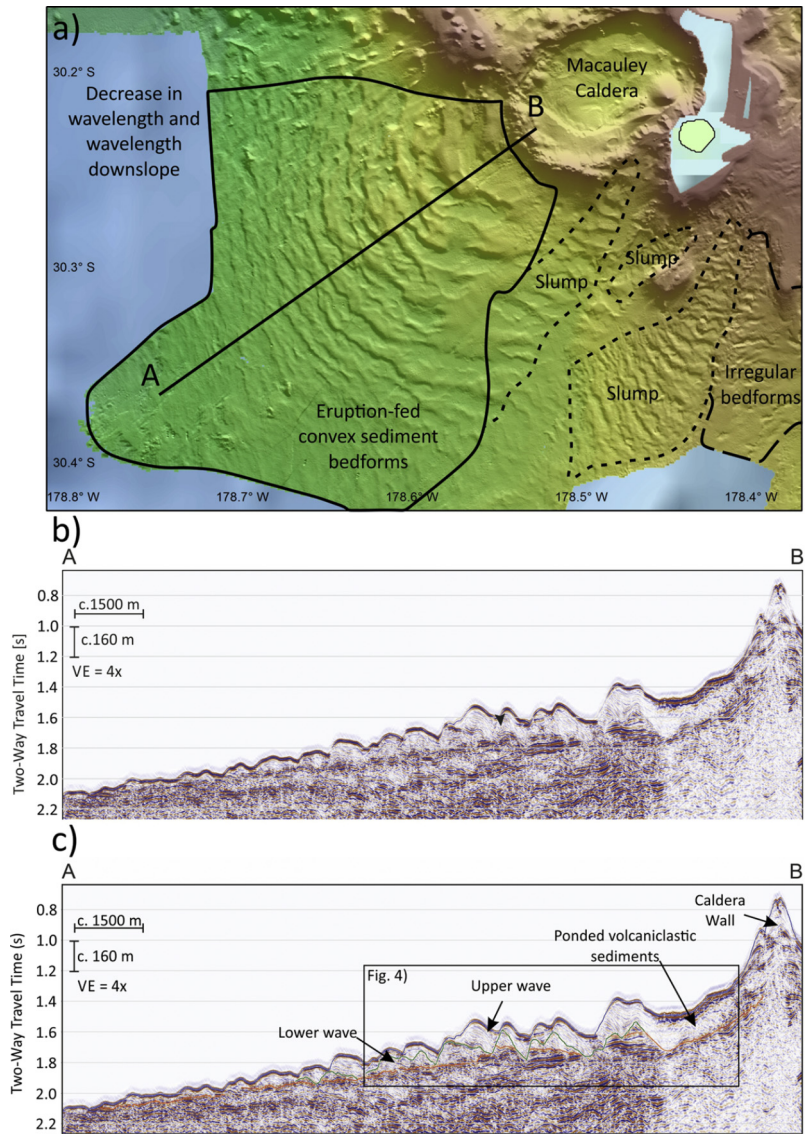

Fig. 3. Eruption-fed bedforms offshore Macauley Volcano. a) Bathymetry of the southwest flank of the submarine Macauley Caldera showing seafloor bedforms of different origins. b) Extract of multi-channel seismic line, whose location is donated by A–B in panel a. c) Interpretation of the seismic line shows an unconformable surface at the base of the sediment waves (orange line) and the lower and upper sets of sediment waves separated by an inferred surface (green line).

the sedimentary bed. The bedform architecture results from sediment deposition occurring mainly on the upcurrent flank of each bedform, while erosion and lower rates of erosion dominate the downstream flank. The bedforms migrate upslope and prograde upcurrent as a result of these flows. Second, the observed bedforms could be a consequence of sediment density flows unrelated to an eruption. Third, they could be the surface expression of a single (or multiple) submarine landslide(s), each bedform resulting from the downslope movement of material. In this case the internal architecture of the bedforms is a consequence of the deformation of material contained within each slide block during its downslope transition.

Of these possible emplacement mechanisms, we interpret the bedforms to the southwest of Macauley Volcano to have originated as a consequence of eruption-fed density derived from eruption column collapse; the bedforms originating as a consequence of instabilities between a flow and the sedimentary bed. We favour this interpretation for the following reasons.

1) The bedform crests are radially extensive and sub-parallel to the caldera rim which fan out in a regular pattern, as might be expected for voluminous, poorly-confined sediment density flows formed by radial collapse of an eruption column.

2) The bedforms do not originate from a distinct headscarp, nor are they strongly confined by submarine valleys, as might be expected for a landslide.

3) Perhaps most importantly, our interpretation of the regular reflectors incised into the underlying substrate as troughs suggests that these bedforms are not related to landslide activity. Were these bedforms related to landslides, translation of material would result in deformation within each slide block and thus may produce the internal reflector patterns observed (Hampton et al., 1996). It would, however, be unlikely to periodically erode into the substrate below the failure surface.

4) No compressional zone is identifiable on the bathymetry or seismic data as might be expected from a landslide.

5) The bedform wavelength and amplitude is similar to that produced by fine-grained and mainly supercritical turbidity currents in non-volcanic settings (see Fig. 1).

6) An origin for the bedforms being generated from sediment density flows that are unrelated to eruptions is discounted. It is not obvious how such energetic flows, which are needed to erode

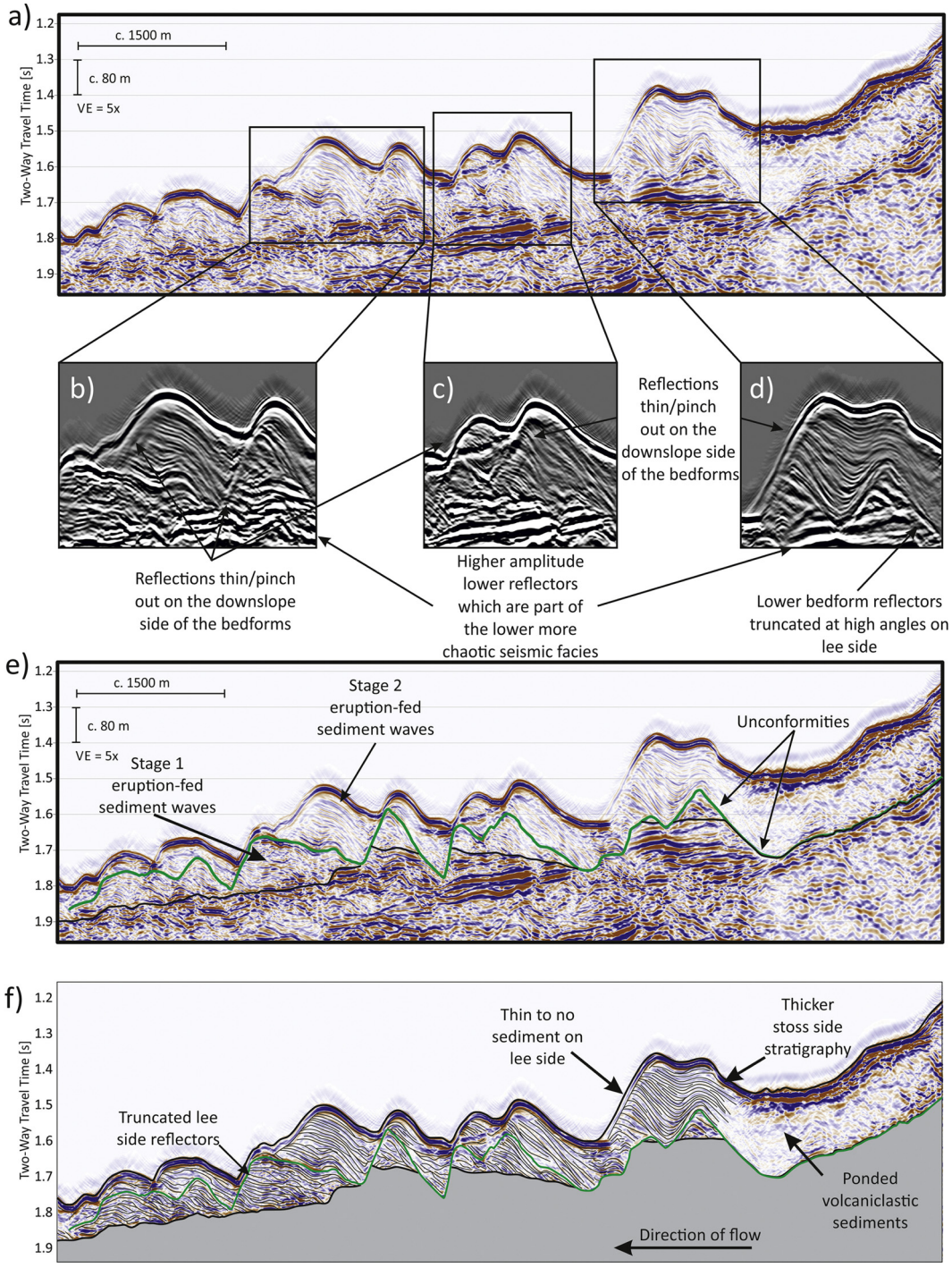

Fig. 4. Detailed extract and interpretation of the multi-channel seismic line in Fig. 3. a) Un-interpreted extract of detailed seismic data from offshore Macauley Volcano. b), c) and d) raw seismic data of bedforms. Images show the base of each bedform is defined by a high amplitude basal reflector. Above the basal reflector each bedform is made up of two sets of internal reflectors with contrasting seismic characteristics. e) Shows the interpreted internal unconformity in each bedform and the interpreted stratigraphic unconformity which separates the sediment waves from the underlying substrate. e) Trace of seismic reflectors visible within the bedforms.

several tens of meters into the subsurface, could have originated from a narrow submerged caldera rim (Fig. 3a). An eruption source is also more likely given the nearby caldera.

4.1.2. Sediment density flow characteristics

Having interpreted sediment density flows as responsible for the emplacement of the observed bedforms, the bedform morphology and internal architecture will now be analysed to suggest bedform type and therefore the possible flow dynamics which resulted in their emplacement (see Fig. 5). The bedforms symmetry and internal architecture suggests that stoss-side deposition and lee-side erosion occurred during their formation. This suggests that the bedforms migrated upstream and thus we can exclude any bedform type which is downstream migrating. This leaves two candidates for the bedforms; anti-dunes and cyclic steps. In comparison to anti-dunes, cyclic steps are considered to generally be longer wavelength and more asymmetrical bedforms (Cartigny et al., 2011). They are characterised by depositional subcritical flow over their stoss side and erosive supercritical flow over their lee side. The systematic transition between the two flow states is char-

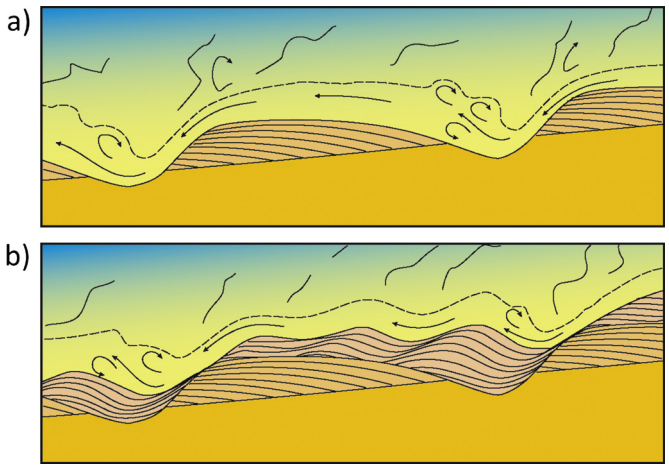

Fig. 5. a) and b) Section-view cartoons showing the envisaged formation of bedforms beneath eruption-fed density flows flowing from right to left. a) Cartoon shows morphology and internal structures of suggested cyclic steps that imply upslope migration of the bedforms under high Froude numbers. b) Morphology and internal structures of shorter more symmetrical bedforms, which are more characteristics of a series of anti-dunes.

acterised by a hydraulic jump (Kostic and Parker, 2006). Meanwhile anti-dune bedforms form in phase (i.e. the flow elevation mimics the bed elevation) with surface waves in a supercritical flow (Cartigny et al., 2011).

In the lower part of the stratigraphy (see Fig. 4), the internal reflectors of the longer wavelength bedforms are strongly asymmetric. In contrast, the internal reflectors in the upper part of the stratigraphy are shorter and more symmetrical. We therefore interpret this geometry to be representative of cyclic step deposits overlain by a series of anti-dunes. Superposition of more symmetrical bedforms on top of longer cyclic steps as has been previously observed in experiments (Cartigny et al., 2014) and modelling (Kostic, 2014). This superposition often reflects a drop in Froude number through time (Cartigny et al., 2014; Zhong et al., 2015). However, in both cases the bedform emplacing flow is dominated by supercritical flow conditions.

Distally, the boundary between the two sets of waves is not resolvable, and the wavelength and wave height decrease away from source (Fig. 2b). This may indicate that sediment concentration, grain size, and/or velocity decreased with distance, reducing the flow's ability to modify the seafloor.

4.1.3. Attributing the sediment density flow to an eruption

Seafloor sampling reveals the uppermost sequence of the sediment wave fields offshore Macauley Island is covered by pumice clasts from multiple eruptions (Barker et al., 2012, 2013). Interestingly, Sandy Bay Tephra compositions were not identified, indicating that at least part of the uppermost stacked planar bedded seismic reflectors (Fig. 2) were not related to the 5.7 ka eruption. Current seismic data suggests a maximum burial depth of a few tens of meters below the seafloor. However, coring and further geochemical analyses will be required to resolve the exact post-climactic eruption sediment thickness and the timing of the eruption(s) that generated the conspicuous wave fields.

4.2. Submarine landslides – Raoul Island

The submarine flanks of Raoul Island are characterised by large areas of wavy seafloor morphology (Figs. 2 and 6). A series of bedforms occur to the west and south of the Island. Each bedform train contains at least 30 individual bedforms. These bedforms have concave or linear crests when analysed in planform (Fig. 6). Each bedform train originates at an arcuate headwall located near to the shelf break, extends downslope for ∼10 km, and occur on relatively steep slopes (5°). They are confined to a zone that is 0.5–2 km wide and have sharp lateral boundaries. Individual bedforms are strongly asymmetrical (the upslope limb being 1.65 times longer than the downslope limb) with wavelengths of ∼650 m and heights up to 80 m in proximal areas. Distally, the bedforms become more symmetrical (the upslope limb is 1.09 times longer than the downslope limb) and smaller in height (10 m).

The seismic data from the bedforms offshore Raoul Island (Fig. 6b, c) are more chaotic than those seen from the Macauley Volcano bedforms (Figs. 3 and 4). This is partly a consequence of the Raoul seismic line not being perfectly perpendicular to the bedform crests, as was the case for Macauley. Although the noise within the Raoul seismic data makes it difficult to define internal layering, these bedforms do not clearly exhibit the internal reflectors visible in the Macauley Volcano seismic data. Instead, a seismic transect from the western slope of Raoul Island shows a chaotic seismic unit which is bounded at its base by an interpreted scoop-shaped basal surface which truncates well-bedded, seaward-dipping planar stratigraphy beneath. The chaotic seismic unit is interpreted as probable back-rotated stratigraphy, dissected by inferred normal faults. A second basal scoop-shaped surface is also visible suggesting that the one chaotic unit is made of two separate units. The end of the shear surface cannot, however, be defined. Some of the Raoul Island bedforms end in a toe-shaped area of positive bathymetric relief, which is ∼40 m higher than the surrounding seafloor. The greater symmetry of bedforms in the distal parts of these bedform fields may also be a consequence of the compression of sediment in these locations as a consequence of landslide processes.

4.2.1. Emplacement mechanism

The geomorphology and seismic stratigraphy of these bedforms is consistent with that of previously described submarine landslides (Hampton et al., 1996; Shea et al., 2008; Watt et al., 2014). It could be proposed that these bedforms were generated by eruption-fed density flows, which were relatively thin and thus confined within gullies. Equally, it has previously been proposed that small mass-wasting events have led to the formation of crescent-shaped bedforms through the downslope evolution of these flows, such as offshore volcanoes in the Aeolian Archipelago (Romagnoli et al., 2013; Casalbore et al., 2014a, 2014b). However, it is likely that eruption-fed density flows would be less confined than the presented examples and would lead to a gradual transition to overbank bedforms not seen here. Some of these bedforms might also originate via turbidity currents initiated at the shelf edge by non-eruptive processes (cf. Hughes Clarke, 2016), although the limited hydrologic system of Raoul Island prevents large-scale fluvial input to the ocean. Nevertheless the abrupt initiation of the bedforms at a distinct head scarp favours a landslide origin, and the scale of these bedforms is larger than those formed by non-volcanic density flows in similarly confined settings, where bedforms typically have wavelengths of $<$200 m, and heights of $<$10 m (Symons et al., 2016).

We interpret these bedform trains as most likely the result of slope failure for the following reasons.

1) Bedforms trains originate abruptly from a distinct arcuate headwall, which is most consistent with landslides.

2) The bedform trains are laterally confined in valleys, and absent on intervening interfluves.

3) There is some evidence in the seismic data for backward-rotated blocks.

4) A toe-shaped area of positive bathymetric relief exists at the base of the slope which we interpret to represent the compressional zone exhibited by other known submarine landslides

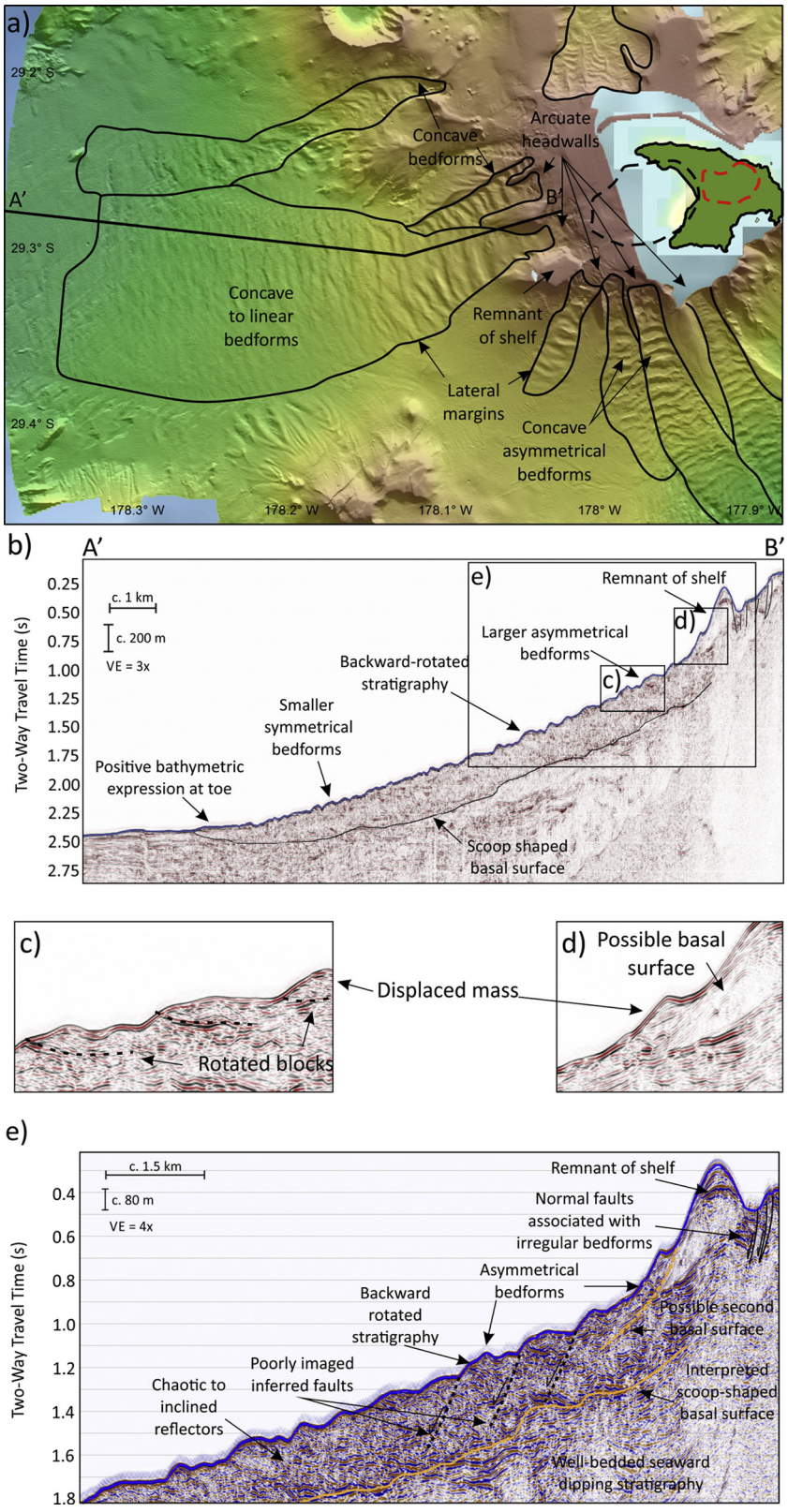

Fig. 6. Landslide-related bedforms on the submarine southwestern flank of Raoul Island. a) Bathymetry map showing bedforms related to slope failure (black polygons). b) Extract of multi-channel seismic line, whose location is shown by A′–B′ in part a). c) and d) detailed extract of individual bedforms. Figures show possible rotated blocks, displaced mass and a possible basal sliding surface. e) Detailed extract of line A′–B′ showing the internal architecture of the bedforms. Although poorly imaged, the downslope limbs of the bedforms are inferred to be associated with listric faults that are connected to a basal surface.

(Hampton et al., 1996). The greater symmetry of bedforms in the distal parts of these bedform fields may also be a consequence of the compression of sediment in these locations as a consequence of landslide processes.

Together this evidence suggests that the identified bedforms are the result of slope failure. However, it must be acknowledged that eruption-fed density flows cannot be ruled out as the formative process and therefore further higher resolution seismic data is needed to be certain (Table 1).

5. Discussion

5.1. A global comparison of volcanic island bedforms

Although spectacular, the bedform fields observed on the flanks of Macauley Volcano and Raoul Island are not unique. Bedform fields have been observed on the submarine flanks of volcanic islands worldwide in other subduction zone, collision zone and hot spot settings (see supplementary Table 1). These sites include Stromboli (Kidd et al., 1998), Canary Islands (Wynn et al., 2000), the Bismark Volcanic Arc (Hoffmann et al., 2008; Silver et al., 2009), the West Mariana Arc (Gardner, 2010), South Sandwich Islands (Leat et al., 2010), Reunion Island (Sisavath et al., 2011) and the Madeira Archipelago (Quartau et al., 2018). Nonetheless it has often been difficult to unambiguously infer the origin of these bedforms (Quartau et al., 2018). The following section will therefore compare the bedform fields observed offshore Macauley Volcano and Raoul Island with other identified bedform fields and outline a set of general criteria for determining bedform origin.

5.1.1. Are Macauley Volcano and Raoul Island bedforms unique?

Macauley Volcano and Raoul Island bedforms reported in this study have wave heights ranging from 10 m to 140 m and wavelengths of 250 m to 2000 m. Globally, reported bedform wave heights have been reported ranging from 2.5 m to 340 m (see Fig. 1; Babonneau et al., 2013; Leat et al., 2013). Globally, wavelengths vary between 10 m and 3.5 km (Moore and Chadwick, 1994; Ollier et al., 1998). Although larger than average (see Fig. 1), the wave heights and lengths reported in this study are therefore fairly typical of bedform sizes reported in other locations.

The planview morphology of the Macauley and Raoul bedforms varied from convex to concave with some classified as wavy (see Fig. 2 and Table 1). Their setting was also variable; some bedform fields were confined between sidewalls (see Fig. 6) whilst others remained unconfined (Fig. 3). The confined bedforms were often associated with a distinct upper headscarp. The morphology of these features is similar to those seen on other volcanic islands. The northern flanks of La Palma exhibit a series of unconfined convex, sinuous and bifurcating bedforms which are parallel to the regional slope (Wynn et al., 2000). They also exhibit internal architectures similar to those described for the bedforms offshore Macauley Island (see Section 3). In contrast, the flanks of Montagu and Bristol Islands are characterised by laterally confined bedforms near to the shelf edge which are associated with arcuate headwalls (Leat et al., 2010, 2013). These bedforms are similar to those interpreted as landslide sourced offshore Raoul Island (see Section 3). The bedforms reported in this study are therefore fairly typical of bedforms seen on other volcanic islands and are thought to be the result of similar processes. Observations/interpretations from Macauley and Raoul should therefore be able to inform the interpretation of other volcanic island bedforms.

One specific type of submarine bedform field type observed elsewhere is, however, absent from Macauley Volcano and Raoul Island. On a number of large volcanic islands (e.g. Reunion, Madeira etc.) bedforms associated with the mouths of fluvial systems have been identified (Babonneau et al., 2013; Lebas et al., 2011; Quartau et al., 2018). A consequence of sediment gravity flows related to fluvial discharge and deposition of sediment rather than volcanic activity, the wave height and wavelength of these bedforms is limited compared to their volcanically sourced counterparts. They are also found in association with deep-sea fan systems (Sisavath et al., 2011).

5.1.2. General criteria for determining bedform origin

The presented bathymetry and seismic data in this study suggests that widespread bedforms that fan out radially from a caldera suggest eruption-fed density flows (i.e. Type 1 bedforms in Table 1), whereas a distinct upper headscarp conversely favours a landslide origin. The strongest evidence for eruption-fed density flows comes from seismic data that can resolve internal layering within bedforms (Fig. 4b). Where such layering indicates upslope migration, it indicates formation through supercritical density flows. Rotation of planar-bedded blocks within a landslide can also form up-slope dipping reflectors, thus continuous internal reflectors are needed to preclude a landslide origin (Lee et al., 2002). Detailed seismic data is thus critical for determining the origin of bedforms with confidence, as was also found for studies of bedforms in non-volcanic settings (Lee et al., 2002). Although difficult to obtain due to the coarseness of volcanic sediment (Jutzeler et al., 2014b), sediment cores may increase confidence in how bedforms originate, especially if dating shows the bedforms are coeval with a known subaerial eruption.

5.1.3. Applying the criteria to bedforms from other volcanic islands

From our observations of bedforms offshore Macauley Volcano and Raoul Island, we therefore propose general criteria for understanding the origin of such bedforms (Fig. 7 and Table 1). To assess the applicability of these criteria, we now consider bedforms offshore from the South Sandwich Islands and New Britain.

Originally reported by Hoffmann et al. (2008, 2011), the flanks of Dakataua Caldera and Kimbe Bay in the New Britain Arc (Figs. 8a and 8b) are characterised by bedforms similar to those described on Macauley Volcano. Here, wavelengths range from 500 to 3700 m, and heights from 10 to 100 m. The bedforms are mostly asymmetrical (steeper and shorter lee sides) and decrease in wavelength downslope. Chirp sub-bottom data through the Kimbe Bay wavefield suggests thicker sediment packages on the upslope limb of waves and upslope migrating sediment packages (Hoffmann et al., 2008), therefore similar to those identified as Type 1 (eruption-fed in Table 1).

The flanks of the Candlemas Islands and Zavodovski Island (South Sandwich Arc) are characterised by bedforms originating at arcuate headwalls, and are laterally confined on the upper slope (Figs. 8c and 8d). These bedforms have lengths from 830 to 2500 m, and heights from $<$10 to 150 m (Leat et al., 2010). The bedforms observed offshore the Candlemas Islands and nearby Adventure Volcano (Leat et al., 2013) are similar to those identified as landslide-generated offshore Raoul Island and can therefore be categorised as Type 2 (due to landslides) in Table 1. The origin of bedforms offshore Zavodovski Island is harder to ascertain. Bedforms to the east of Zavodovski originate from headwalls and are confined within gullies suggesting a landslide origin (Type 2 in Table 1). However, the bedform shape changes with distance offshore from concave to convex in some locations. Moreover, shallow seismic data also shows a veneer of downslope prograding sediments containing internal reflectors, suggesting downslope movement of sediment by density flows (Leat et al., 2010). Overbank sediment deposits have also been identified (Leat et al., 2010). The observed bedforms could therefore be interpreted as a consequence of initial mass-wasting (landslide) events followed by eruption-fed density flows thus exhibiting both Type 1 and Type 2 features (Table 1).

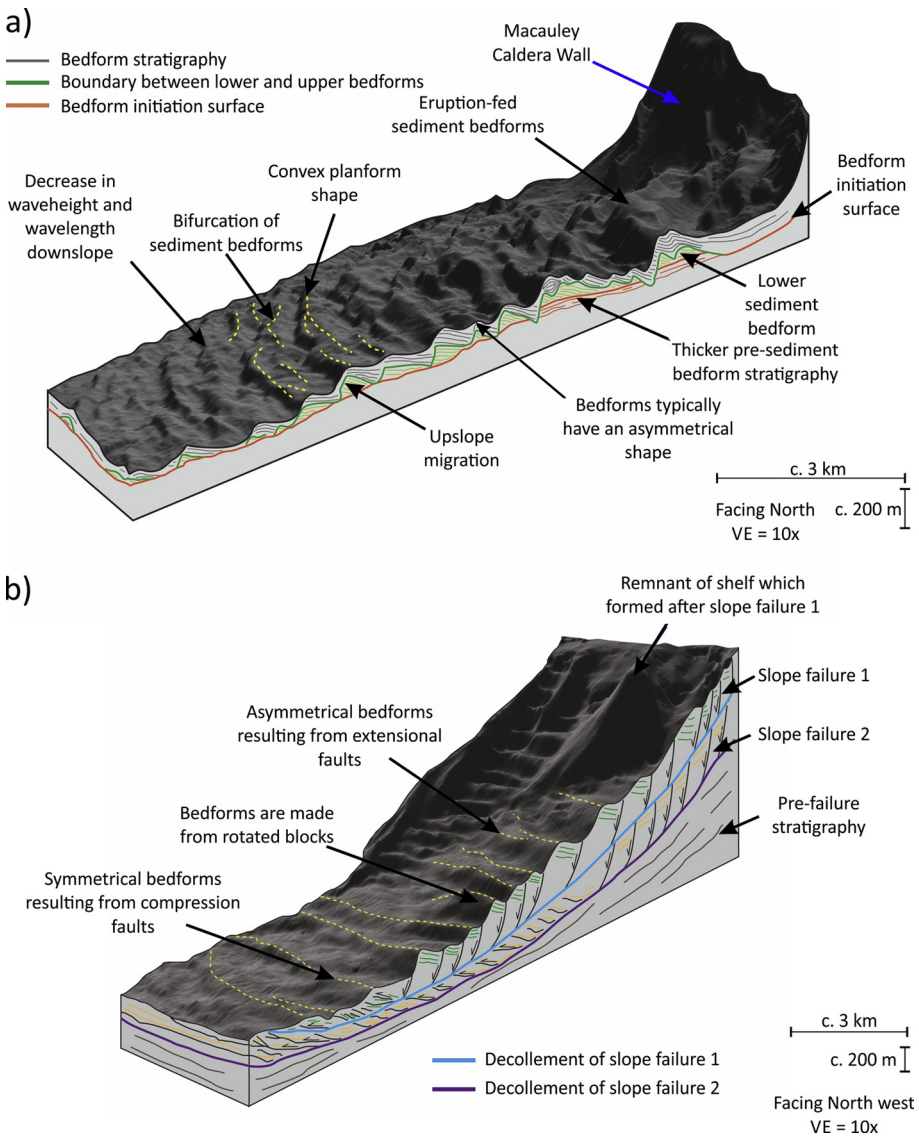

Fig. 7. Summary of observations enabling the identification of bedforms resulting from eruption-fed density flows (type 1) and landslides (type 2), as outlined in Table 1. a) Eruption-fed bedforms on the south-western flank of Macauley Volcano (Fig. 2). b) Landslide-generated bedforms on the western flank of Raoul Island (Fig. 3). The seafloor in a) and b) is a 3D representation of the hill-shaded bathymetry.

These examples demonstrate that it is possible to use the general criteria set out in Table 1 as a means to make initial assessment of the processes resulting in different volcanic island flank morphologies. However, the complexity shown offshore Zavodovski Island indicates that caution is required in terms of prescribing specific formation processes in these locations without suitably detailed seismic data in addition to high resolution bathymetric data.

5.2. Comparison between submarine and subaerial volcanic bedforms

There are strong differences in morphology of volcanic bedforms between subaerial and submarine domains. These morphological discrepancies between subaerial and submarine deposits reflect the different hydrodynamic properties of these flows, subject to the density of the interstitial fluid (gas against water). Another influencing factor may be the slope morphology, coarseness and composition of the substrate.

5.2.1. Bedforms from eruption-fed density flows

Pyroclastic density currents produced by subaerial volcanism create deposits that range from massive, to non to poorly-stratified deposits (Sparks, 1976), and to deposits recording more dilute conditions, forming sets of dunes and anti-dunes (Sigurdsson et al., 1987; Brown and Branney, 2004). However, subaerial-deposited bedforms do not match the size and extent of the submarine bedforms presented in this study. Dilute pyroclastic density current deposits have bedform heights of <5–10 m and wavelengths reaching several hundred meters (Brown and Branney, 2004). In contrast, the submarine bedforms described here have heights of 10–150 m, and wavelengths can be up to 1700 m and are therefore at least one order of magnitude greater. Dunes formed by dilute pyroclastic density currents can extend across areas up to ~150 km^2 (Sigurdsson et al., 1987), but can be much more localised (Brown and Branney, 2004), and much less extensive than the studied submarine bedforms (>400 km^2).

Large-magnitude silicic eruptions (i.e. Plinian in the subaerial realm) produce high-flux, sustained pyroclastic density currents that can last hours to days (Wolfe and Hoblitt, 1996; Maeno and Imamura, 2011). Under such conditions, voluminous sediment input in the ocean may be continuous for long periods of time, favouring instalment of prolonged sedimentation conditions on the seafloor. This eruptive behaviour is in strong contrast with instan-

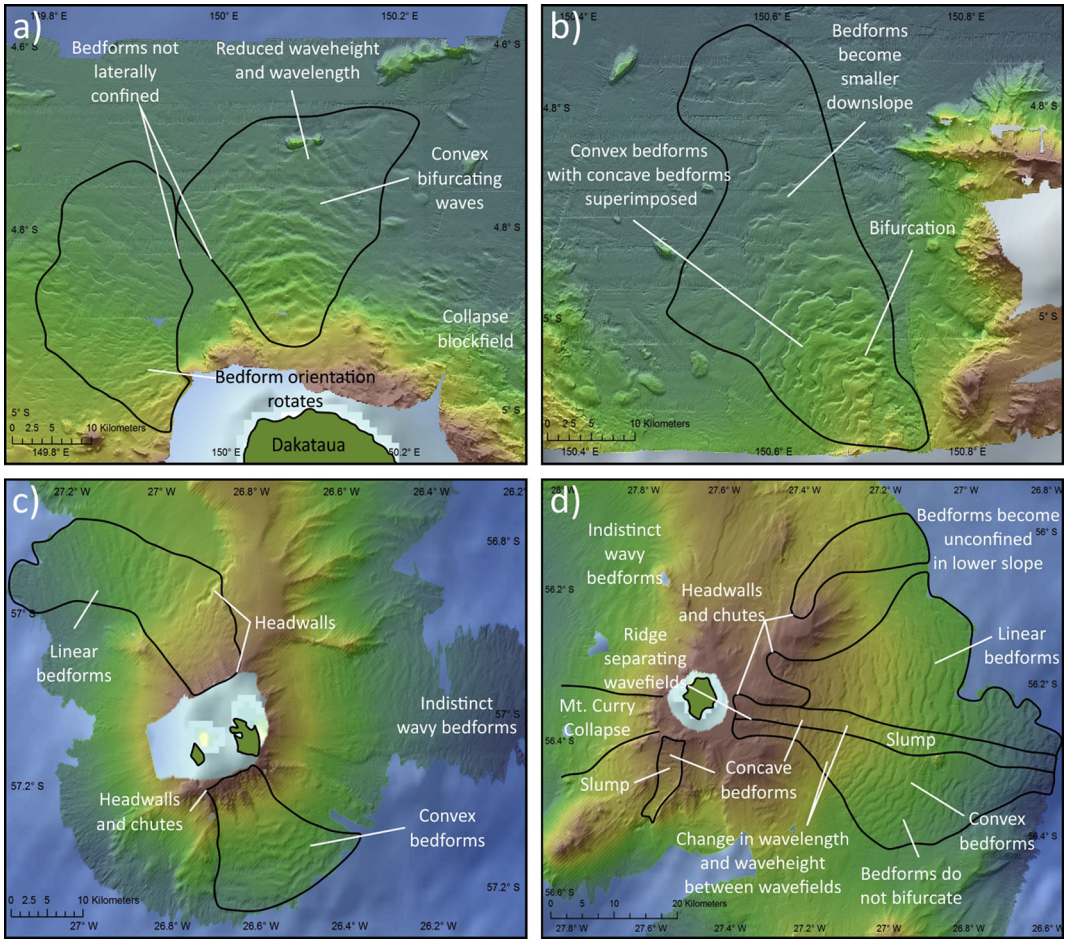

Fig. 8. Multibeam bathymetric maps from offshore New Britain (50 m grid resolution) in the Pacific Ocean (Hoffmann et al., 2008, 2011) and the South Sandwich Islands (100 m grid resolution) in the South Atlantic Ocean (Leat et al., 2010). a) Dakataua Caldera and b) Kimbe Bay are offshore New Britain. c) Candlemas Islands and d) Zavodovski Island are in the South Sandwich Arc. Bedforms offshore Dakataua Caldera and Kimbe Bay are mostly asymmetrical and decrease in wavelength and wave height downslope. These bedforms are therefore consistent with eruption-fed density flows. Bedforms offshore the Candlemas Islands and Zavodovski are mainly associated with arcuate headwalls at the shelf edge, are confined within gullies within the upper slope, and wavelength and waveheight decreases with distance offshore. These characteristics suggest a landslide origin (Table 1). Bedforms east of Zavodovski may also have been the result of later eruption-fed density flows (see text for details). In all cases, detailed seismic data are needed for unambiguous identification of bedforms that are produced by landslides and eruption-fed density flows (cf. Lee et al., 2002).

taneous, essentially mass-wasting events such as collapse of an active lava dome or sector collapse (Voight et al., 2002; Trofimovs et al., 2006, 2008), which are associated with gravitational instabilities or vulcanian explosions. Moreover, volumes of transported sediment through lava dome collapses are commonly less voluminous. It is therefore difficult to use literature examples of such collapses to infer hydrodynamic properties in sustained volcaniclastic density flows. Offshore Montserrat, the density flow deposits derived from dome and sector collapses lack bedforms, which we interpret as resulting from rapid accumulation of sediment from short-lived, non-sustained events (Trofimovs et al., 2006, 2008).

Here, we propose that eruption-fed density flows produce larger and more extensive bedforms in submarine slope settings for the following reasons. First, submarine density flows have smaller density contrasts between their interstitial fluid (seawater) and the transported sediment than for subaerial pyroclastic density currents (air and magmatic gases). This low density contrast in submarine density flows favours supercritical flows (Kostic and Parker, 2006; Cartigny et al., 2014). Moreover, this implies that submarine density flows are slower than their subaerial equivalent, and respond more slowly to changes in slope, such as on the stoss and lee slopes of bedforms (Gray et al., 2006). Such hydrodynamic characteristics lead to formation of larger and more extensive bedforms on underwater slopes (Gray et al., 2006). The small density contrast between particles and seawater also induces slower settling rates of grains (Cashman and Fiske, 1991; Jutzeler et al., 2015), which favours suspension and longer runouts, and hence more extensive bedform fields.

Second, bedform development is strongly affected by the concentration of particles within the lowermost part of the flow. For example, pyroclastic block-and-ash flows (formed by collapse of an active lava dome) often contain a dense granular layer at their base, which is typically confined within topography; it is overlain by dilute pyroclastic density currents (surges) that can travel much further (Calder et al., 1999). Sediment settles more rapidly in air than in water, and this favours the generation of dense near-bed flows on land (Breard et al., 2016) rather than underwater (Sohn, 1997). Bedforms produced by such stratified flows are significantly shorter (Cartigny et al., 2014; Postma and Cartigny, 2014; Symons et al., 2016). Future modelling is necessary to test how these various factors may combine to favour bedform generation in submarine settings.

5.2.2. *Bedforms associated with volcanic landslides*

Sector collapse of a volcano triggers debris avalanches, which can form hummocks and Toreva blocks in their deposits (e.g. Crandell et al., 1984), but their morphology differ from results of this study. The Type 2 bedforms (Table 1) that we ascribe as most likely originating from landslides (Figs. 6 and 7) differ markedly from the hummocky terrain typically associated with

subaerial debris avalanches. Submarine landslide hummocks are chaotic and tend to lack elongate crests; they are not so regularly distributed as the submarine bedforms described here (Watt et al., 2015). Debris avalanches can produce rotated Toreva blocks with linear crests (e.g. Clavero et al., 2002); however, the regular spacing and linear crests of the Type 2 submarine bedforms more closely resembles the morphology of non-volcanic submarine landslides, such as the Eureka Slump offshore Alaska or the Storegga Slide offshore Norway (e.g. Hampton et al., 1996; Micallef et al., 2008). Submarine linear crests are created in response to normal faulting by extension along a seafloor-parallel detachment surface, which produces rows of tilted fault blocks (e.g. Micallef et al., 2008). It records situations in which the failed material does not disintegrate fully, and where marine sediment provides extensive weak layers for regional detachment. The submarine landslide morphology discussed also differs from many previously described submarine landslide, such as deeper-seated and larger failures offshore from the Canary Islands (Masson et al., 2006) in which the landslide material has more fully disintegrated.

6. Conclusions

Here, we present two detailed marine geophysical datasets from Macauley and Raoul Islands in the Kermadec Arc, which include detailed seismic sub-seafloor profiles through bedforms. Some bedform fields result from eruption-fed submarine density flows. These eruption-fed bedforms are radially extensive around a caldera structure, and seismic profiles show that bedforms migrated up-slope. However, other types of bedform represent rotated blocks in submarine landslides. We therefore propose a series of generally applicable criteria for distinguishing bedforms formed by eruption-fed density flows and landslides (Table 1). As in non-volcanic settings, it may be necessary to collect and analyse detailed seismic data to avoid ambiguity.

Submarine density flows derived from sustained silicic explosive eruptions produce larger and more extensive bedforms than pyroclastic density currents, their subaerial equivalent. This is mainly due to the lower density difference between the transported sediment and the interstitial fluid. Relatively slow settling of sediment in water favours formation of bedforms, whereas fast settling of pyroclastic density currents in air favour formation of dense basal layers and flow stratification. Moreover, the reduced density difference causes a slower response of submarine flows to changes in seafloor gradients generating large and extensive bedforms. Bedform occurrence and geometry suggests that the dynamics of submarine and subaerial mass flows are markedly different.

Acknowledgements

We would like to thank the New Zealand National Institute of Water and Atmospheric Research (NIWA), Dr. Gary Hoffman, Dr. Eli Silver and Dr. Phil Leat for providing access to the fantastic datasets presented as part of this study. We thank the editor Tamsin Mather, two anonymous reviewers and M. Perillo for their constructive reviews that greatly improved the manuscript. E. Pope was supported by the UK NERC Arctic Research Programme under the project on whether climate change increases the landslide-tsunami risk to the UK (NE/K00008X/1). M. Cartigny was supported in part by the NERC grant (NE/M017540/1), 'Co-ordinating and pump-priming international efforts for direct monitoring of active turbidity currents at global test sites'.

Appendix A. Supplementary material

Supplementary material related to this article can be found online at https://doi.org/10.1016/j.epsl.2018.04.020.

References

Allen, S.R., Freundt, A., Kurokawa, K., 2012. Characteristics of submarine pumice-rich density current deposits sourced from turbulent mixing of subaerial pyroclastic flows at the shoreline: field and experimental assessment. Bull. Volcanol. 74, 657–675.
Allen, S.R., McPhie, J., 2009. Products of neptunian eruptions. Geology 37, 639–642.
Babonneau, N., Delacourt, C., Cancouët, R., Sisavath, E., Bachèlery, P., Mazuel, A., Jorry, S.J., Deschamps, A., Ammann, J., Villeneuve, N., 2013. Direct sediment transfer from land to deep-sea: insights into shallow multibeam bathymetry at La Réunion Island. Mar. Geol. 346, 47–57.
Barker, S.J., Rotella, M.D., Wilson, C.J.N., Wright, I.C., Wysoczanski, R.J., 2012. Contrasting pyroclast density spectra from subaerial and submarine silicic eruptions in the Kermadec arc: implications for eruption processes and dredge sampling. Bull. Volcanol. 74, 1425–1443.
Barker, S.J., Wilson, C.J.N., Baker, J.A., Millet, M.-A., Rotella, M.D., Wright, I.C., Wysoczanski, R.J., 2013. Geochemistry and petrogenesis of silicic magmas in the intra-oceanic Kermadec arc. J. Petrol. 54, 351–391.
Branney, M.J., Kokelaar, B.P., 2002. Pyroclastic Density Currents and the Sedimentation of Ignimbrites. Geological Society of London, pp. 1–152.
Breard, E.C.P., Lube, G., Jones, J.R., Dufek, J., Cronin, S.J., Valentine, G.A., Moebis, A., 2016. Coupling of turbulent and non-turbulent flow regimes within pyroclastic density currents. Nat. Geosci. 9, 767–771.
Brown, R.J., Branney, M.J., 2004. Bypassing and diachronous deposition from density currents: evidence from a giant regressive bed form in the Poris ignimbrite, Tenerife, Canary Islands. Geology 32, 445–448.
Busby, C.J., Tamura, Y., Blum, P., Guèrin, G., Andrews, G.D.M., Barker, A.K., Berger, J.L.R., Bongiolo, E.M., Bordiga, M., DeBari, S.M., Gill, J.B., Hamelin, C., Jia, J., John, E.H., Jonas, A.-S., Jutzeler, M., Kars, M.A.C., Kita, Z.A., Konrad, K., Mahony, S.H., Martini, M., Miyazaki, T., Musgrave, R.J., Nascimento, D.B., Nichols, A.R.L., Ribeiro, J.M., Sato, T., Schindlbeck, J.C., Schmitt, A.K., Straub, S.M., Mleneck-Vautravers, M.J., Yang Yang, A., 2017. The missing half of the subduction factory: shipboard results from the Izu rear arc, IODP Expedition 350. Int. Geol. Rev. 59, 1677–1708.
Calder, E.S., Cole, P.D., Dade, W.B., Druitt, T.H., Hoblitt, R.P., Huppert, H.E., Ritchie, L., Sparks, R.S.J., Young, S.R., 1999. Mobility of pyroclastic flows and surges at the Soufriere Hills Volcano, Montserrat. Geophys. Res. Lett. 26, 537–540.
Cartigny, M.J.B., Postma, G., van den Berg, J.H., Mastbergen, D.R., 2011. A comparative study of sediment waves and cyclic steps based on geometries, internal structures and numerical modeling. Mar. Geol. 280, 40–56.
Cartigny, M.J.B., Ventra, D., Postma, G., Den Berg, J.H., 2014. Morphodynamics and sedimentary structures of bedforms under supercritical-flow conditions: new insights from flume experiments. Sedimentology 61, 712–748.
Cas, R.A.F., Wright, J.V., 1991. Subaqueous pyroclastic flows and ignimbrites: an assessment. Bull. Volcanol. 53, 357–380.
Casalbore, D., Romagnoli, C., Bosman, A., Chiocci, F.L., 2014a. Large-scale seafloor waveforms on the flanks of insular volcanoes (Aeolian Archipelago, Italy), with inferences about their origin. Mar. Geol. 355, 318–329.
Casalbore, D., Bosman, A., Martorelli, E., Sposato, F.L., Chiocci, F.L., 2014b. Mass wasting features on the submarine flanks of Ventotene volcanic edifice (Tyrrhenian Sea, Italy). In: Krastel, et al. (Eds.), Submarine Mass Movements and Their Consequences, vol. 37, pp. 285–293.
Cashman, K.V., Fiske, R.S., 1991. Fallout of pyroclastic debris from submarine volcanic eruptions. Science 253, 275.
Clavero, J., Sparks, R.S.J., Huppert, H., Dade, W., 2002. Geological constraints on the emplacement mechanism of the Parinacota debris avalanche, northern Chile. Bull. Volcanol. 64, 40–54.
Crandell, D.R., Miller, C.D., Glicken, H.X., Christiansen, R.L., Newhall, C.G., 1984. Catastrophic debris avalanche from ancestral Mount Shasta volcano, California. Geology 12, 143–146.
Gardner, J.V., 2010. The West Mariana Ridge, western Pacific Ocean: geomorphology and processes from new multibeam data. Geol. Soc. Am. Bull. 122, 1378–1388.
Gray, T.E., Alexander, J., Leeder, M.R., 2006. Longitudinal flow evolution and turbulence structure of dynamically similar, sustained, saline density and turbidity currents. J. Geophys. Res., Oceans 111.
Hampton, M.A., Lee, H.J., Locat, J., 1996. Submarine landslides. Rev. Geophys. 34, 33–59.
Head, J.W., Wilson, L., 2003. Deep submarine pyroclastic eruptions: theory and predicted landforms and deposits. J. Volcanol. Geotherm. Res. 121, 155–193.
Hoffmann, G., Silver, E., Day, S., Driscoll, N., Orange, D., 2011. Deformation versus deposition of sediment waves in the Bismarck Sea, Papua New Guinea. Mass-transport deposits in deepwater settings. SEPM Spec. Publ. 96, 455–474.
Hoffmann, G., Silver, E., Day, S., Morgan, E., Driscoll, N., Orange, D., 2008. Sediment waves in the Bismarck volcanic arc, Papua New Guinea. Spec. Pap., Geol. Soc. Am. 436, 91–126.
Hughes Clarke, J.E., 2016. First wide-angle view of channelized turbidity currents links migrating cyclic steps to flow characteristics. Nat. Commun. 7, 11896.
Hunt, J.E., Wynn, R.B., Talling, P.J., Masson, D.G., 2013. Turbidite record of frequency and source of large volume (>100 km^3) Canary Island landslides in the last 1.5 Ma: implications for landslide triggers and geohazards. Geochem. Geophys. Geosyst. 14, 2100–2123.

Jutzeler, M., McPhie, J., Allen, S.R., 2014a. Submarine eruption-fed and resedimented pumice-rich facies: the Dogashima Formation (Izu Peninsula, Japan). Bull. Volcanol. 76, 867.
Jutzeler, M., McPhie, J., Allen, S.R., Proussevitch, A.A., 2015. Grain-size distribution of volcaniclastic rocks, 2: characterizing grain size and hydraulic sorting. J. Volcanol. Geotherm. Res. 301, 191–203.
Jutzeler, M., White, J.D.L., Talling, P.J., McCanta, M., Morgan, S., Le Friant, A., Ishizuka, O., 2014b. Coring disturbances in IODP piston cores with implications for offshore record of volcanic events and the Missoula megafloods. Geochem. Geophys. Geosyst. 15, 3572–3590.
Kidd, R.B., Lucchi, R.G., Gee, M., Woodside, J.M., 1998. Sedimentary processes in the Stromboli Canyon and Marsili Basin, SE Tyrrhenian Sea: results from side-scan sonar surveys. Geo Mar. Lett. 18, 146–154.
Kokelaar, P., Busby, C., 1992. Subaqueous explosive eruption and welding of pyroclastic deposits. Science 257, 196–201.
Kostic, S., 2014. Upper flow regime bedforms on levees and continental slopes: turbidity current flow dynamics in response to fine-grained sediment waves. Geosphere 10 (6), 1094–1103.
Kostic, S., Parker, G., 2006. The response of turbidity currents to a canyon–fan transition: internal hydraulic jumps and depositional signatures. J. Hydraul. Res. 44, 631–653.
Le Friant, A., Ishizuka, O., Boudon, G., Palmer, M.R., Talling, P.J., Villemant, B., Adachi, T., Aljahdali, M., Breitkreuz, C., Brunet, M., Caron, B., Coussens, M., Deplus, C., Endo, D., Feuillet, N., Fraas, A.J., Fujinawa, A., Hart, M.B., Hatfield, R.G., Hornbach, M., Jutzeler, M., Kataoka, K.S., Komorowski, J.-C., Lebas, E., Lafuerza, S., Maeno, F., Manga, M., Martinez-Colon, M., McCanta, M., Morgan, S., Saito, T., Slagle, A., Sparks, R.S.J., Stinton, A., Stroncik, N., Subramanyam, K.S.V., Tamura, Y., Trofimovs, J., Voight, B., Wall-Palmer, D., Wang, F., Watt, S.F.L., 2015. Submarine record of volcanic island construction and collapse in the Lesser Antilles arc: first scientific drilling of submarine volcanic island landslides by IODP Expedition 340. Geochem. Geophys. Geosyst. 16, 420–442.
Leat, P.T., Day, S.J., Tate, A.J., Martin, T.J., Owen, M.J., Tappin, D.R., 2013. Volcanic evolution of the South Sandwich volcanic arc, South Atlantic, from multibeam bathymetry. J. Volcanol. Geotherm. Res. 265, 60–77.
Leat, P.T., Tate, A.J., Tappin, D.R., Day, S.J., Owen, M.J., 2010. Growth and mass wasting of volcanic centers in the northern South Sandwich arc, South Atlantic, revealed by new multibeam mapping. Mar. Geol. 275, 110–126.
Lebas, E., Le Friant, A., Boudon, G., Watt, S.F.L., Talling, P.J., Feuillet, N., Deplus, C., Berndt, C., Vardy, M.E., 2011. Multiple widespread landslides during the long-term evolution of a volcanic islands: insights from high-resolution seismic data, Montserrat, Lesser Antilles. Geochem. Geophys. Geosyst. 12, Q05006.
Lee, H.J., Syvitski, J.P.M., Parker, G., Orange, D., Locat, J., Hutton, E.W.H., Imran, J., 2002. Distinguishing sediment waves from slope failure deposits: field examples, including the 'Humboldt slide', and modelling results. Mar. Geol. 192, 79–104.
Lloyd, E.F., Nathan, S., Smith, I.E.M., Stewart, R.B., 1996. Volcanic history of Macauley Island, Kermadec Ridge, New Zealand. N.Z. J. Geol. Geophys. 39, 295–308.
Maeno, F., Imamura, F., 2011. Tsunami generation by a rapid entrance of pyroclastic flow into the sea during the 1883 Krakatau eruption, Indonesia. J. Geophys. Res., Solid Earth 116.
Masson, D.G., Harbitz, C.B., Wynn, R.B., Pedersen, G., Lovholt, F., 2006. Submarine landslides: processes, triggers and hazard prediction. Philos. Trans. R. Soc. Lond. Ser. A 364, 2009–2039.
Micallef, A., Berndt, C., Masson, D.G., Stow, D.A.V., 2008. Scale invariant characteristics of the Storegga Slide and implications for large-scale submarine mass movements. Mar. Geol. 247, 46–60.
Moore, G.J., Chadwick, W.W., 1994. Giant Hawaiian Landslides. Annu. Rev. Earth Planet. Sci. 22, 119–144.
Moorhouse, B.L., White, J.D.L., 2016. Interpreting ambiguous bedforms to distinguish subaerial base surge from subaqueous density current deposits. Depos. Rec. 2, 173–195.
Nishimura, A., Marsaglia, K.M., Rodolfo, K.S., Colella, A., Hiscott, R.N., Tazakl, K., Gill, J.B., Janecek, T., Firth, J., Isiminger-Kelso, M., 1991. Pliocene–Quaternary submarine pumice deposits in the Sumisu rift area, Izu–Bonin arc. In: Fischer, R.V., Smith, G.A. (Eds.), Sedimentation in Volcanic Settings. SEPM, Tulsa, USA.
Ollier, G., Cochonat, P., Lenat, J.F., Labazuy, P., 1998. Deep-sea volcaniclastic sedimentary systems: an example from La Fournaise volcanic, La Reunion Island, Indian Ocean. Sedimentology 45, 293–330.
Postma, G., Cartigny, M.J.B., 2014. Supercritical and subcritical turbidity currents and their deposits—a synthesis. Geology 42, 987–990.
Pyle, D.M., 1995. Mass and energy budgets of explosive volcanic eruptions. Geophys. Res. Lett. 22, 563–566.
Quartau, R., Ramalho, R.S., Madeira, J., Santos, R., Rodriques, A., Roque, C., Carrara, G., da Silveira, A.B., 2018. Gravitational, erosional and depositional processes on volcanic ocean islands: insights from the submarine morphology of Madeira Archipelago. Earth Planet. Sci. Lett. 482, 288–299.
Romagnoli, C., Casalbore, D., Bosman, A., Braga, R., Chiocci, F.L., 2013. Submarine structure of Vulcano volcano (Aeolian Islands) revealed by high-resolution bathymetry and seismo-acoustic data. Mar. Geol. 338, 30–45.
Rotella, M.D., Wilson, C.J.N., Barker, S.J., Cashman, K.V., Houghton, B.F., Wright, I.C., 2014. Bubble development in explosive silicic eruptions: insights from pyroclast vesicularity textures from Raoul volcano (Kermadec arc). Bull. Volcanol. 76, 826.
Shane, P., Wright, I.C., 2011. Late Quaternary tephra layers around Raoul and Macauley Islands, Kermadec Arc: implications for volcanic sources, explosive volcanism and tephrochronology. J. Quat. Sci. 26, 422–432.
Shea, T., de Vries, B.v.W., Pilato, M., 2008. Emplacement mechanisms of contrasting debris avalanches at Volcán Mombacho (Nicaragua), provided by structural and facies analysis. Bull. Volcanol. 70, 899.
Sigurdsson, H., Carey, S.N., Fisher, R.V., 1987. The 1982 eruptions of El Chichon volcano, Mexico (3): physical properties of pyroclastic surges. Bull. Volcanol. 49, 467–488.
Silver, E., Day, S., Ward, S., Hoffmann, G., Llanes, P., Driscoll, N., Appelgate, B., Saunders, S., 2009. Volcano collapse and tsunami generation in the Bismarck volcanic arc, Papua New Guinea. J. Volcanol. Geotherm. Res. 186, 210–222.
Sisavath, E., Babonneau, N., Saint-Ange, F., Bachelery, P., Jorry, S.J., Deplus, C., De Voogd, B., Savoye, B., 2011. Morphology and sedimentary architecture of a modern volcaniclastic turbidite system: the Cilaos fan, offshore La Réunion Island. Mar. Geol. 288, 1–17.
Smith, I.E.M., Stewart, R.B., Price, R.C., 2003. The petrology of a large intra-oceanic silicic eruption: the Sandy Bay Tephra, Kermadec Arc, Southwest Pacific. J. Volcanol. Geotherm. Res. 124, 173–194.
Sohn, Y.K., 1997. On traction-carpet sedimentation. J. Sediment. Res. 67.
Sparks, R.S.J., 1976. Grain size variations in ignimbrites and implications for the transport of pyroclastic flows. Sedimentology 23, 147–188.
Spinewine, B., Sequeiros, O.E., Garcia, M.H., Beaubouef, R.T., Sun, T., Savoye, B., Parker, G., 2009. Experiments on wedge-shaped deep sea sedimentary deposits in minibasins and/or on channel levees emplaced by turbidity currents. Part II. Morphodynamic evolution of the wedge and of the associated bedforms. J. Sediment. Res. 79, 608–628.
Symons, W.O., Sumner, E.J., Talling, P.J., Cartigny, M.J.B., Clare, M.A., 2016. Large-scale sediment waves and scours on the modern seafloor and their implications for the prevalence of supercritical flows. Mar. Geol. 371, 130–148.
Trofimovs, J., Amy, L.A., Boudon, G., Deplus, C., Doyle, E., Fournier, N., Hart, M.B., Komorowski, J.C., Le Friant, A., Lock, E.J., 2006. Submarine pyroclastic deposits formed at the Soufrière Hills volcano, Montserrat (1995–2003): what happens when pyroclastic flows enter the ocean? Geology 34, 549–552.
Trofimovs, J., Sparks, R., Talling, P.J., 2008. Anatomy of a submarine pyroclastic flow and associated turbidity current: July 2003 dome collapse, Soufrière Hills volcano, Montserrat, West Indies. Sedimentology 55, 617–634.
Voight, B., Komorowski, J.C., Norton, G.E., Belousov, A.B., Belousova, M., Boudon, G., Francis, P.W., Franz, W., Heinrich, P., Sparks, R.S.J., 2002. The 26 December (Boxing Day) 1997 sector collapse and debris avalanche at Soufriere Hills volcano, Montserrat. Mem. Geol. Soc. Lond. 21, 363–407.
Watt, S.F.L., Jutzeler, M., Talling, P.J., Carey, S.N., Sparks, R.S.J., Tucker, M., Stinton, A.J., Fisher, J.K., Wall-Palmer, D., Hühnerbach, V., 2015. New insights into landslide processes around volcanic islands from Remotely Operated Vehicle (ROV) observations offshore Montserrat. Geochem. Geophys. Geosyst. 16, 2240–2261.
Watt, S.F.L., Talling, P.J., Hunt, J.E., 2014. New insights into the emplacement dynamics of volcanic island landslides. Oceanography 27, 46–57.
Watt, S.F.L., Talling, P.J., Vardy, M.E., Heller, V., Hühnerbach, V., Urlaub, M., Sarkar, S., Masson, D.G., Henstock, T.J., Minshull, T.A., 2012. Combinations of volcanic-flank and seafloor-sediment failure offshore Montserrat, and their implications for tsunami generation. Earth Planet. Sci. Lett. 319, 228–240.
White, J.D.L., 2000. Subaqueous eruption-fed density currents and their deposits. Precambrian Res. 101, 87–109.
Wolfe, E.W., Hoblitt, R.P., 1996. Overview of the eruptions. In: Newhall, C.G., Pungongbayan, R.S. (Eds.), Fire and Mud: Eruptions and Lahars of Mount Pinatubo, Philippines. Quezon City and University of Washington Press, Seattle, pp. 3–20.
Wright, I.C., Worthington, T.J., Gamble, J.A., 2006. New multibeam mapping and geochemistry of the 30–35 S sector, and overview, of southern Kermadec arc volcanism. J. Volcanol. Geotherm. Res. 149, 263–296.
Wynn, R.B., Masson, D.G., Stow, D.A.V., Weaver, P.P.E., 2000. Turbidity current sediment waves on the submarine slopes of the western Canary Islands. Mar. Geol. 163, 185–198.
Zhong, G., Cartigny, M.J.B., Kuang, Z., Wang, L., 2015. Cyclic steps along the South Taiwan Shoal and West Penghu submarine canyons on the northeastern continental slope of the South China Sea. Geol. Soc. Am. Bull. 127, 804–824.